CrystEngComm

ROYAL SOCIETY OF CHEMISTRY

PAPER

View Article Online
View Journal | View Issue

Cite this: *CrystEngComm*, 2025, **27**, 3128

Twin-like chiral configuration of a calcium oxalate monohydrate mesocrystal regulated with an organic framework in grape leaves†

Ryosuke Tanaka, Hiroto Watanabe, Yuya Oaki and Hiroaki Imai *

Received 10th March 2025,
Accepted 15th April 2025

DOI: 10.1039/d5ce00259a

rsc.li/crystengcomm

Biogenic calcium oxalate monohydrate (COM, $CaC_2O_4{\cdot}H_2O$) needle crystals (raphides) having a pointed tip and two tails are arranged as a bundle in grape leaves. In this work, the specific hierarchical architecture was studied at the micrometric and nanometric scales. Raphides were macroscopically characterized as having a twin-like chiral configuration of COM divided by an organic central wall and covered with an organic enveloping membrane. The COM of the raphides has a mesocrystalline structure that consists of small grains ~10 nm in diameter with a distorted single-crystal nature. The initially produced organic framework was suggested to control the specific crystal growth of COM under the construction of a raphide in a specific cell.

Introduction

In nature, organisms produce various inorganic materials with precisely controlled morphologies from a limited selection of ubiquitous elements—such as calcium, silicon, carbon, and oxygen—under ambient conditions.[1–9] Generally, the morphological design is a critically important aspect of biological mineralization processes with regard to the emergence of specific functions.[3–9]

Calcium oxalate ($CaC_2O_4{\cdot}nH_2O$) is observed in many kinds of plants[10,11] and as a main component of kidney stones,[12] hard objects made from chemicals in urine. Although kidney stones have indefinite morphologies with complicated internal architectures,[12] the shape and microstructure of $CaC_2O_4{\cdot}nH_2O$ are strictly designed in and outside of plant cells.[10,11] However, the key to controlling their morphology and structures has not been clarified sufficiently. In the present study, because of thier sophisticated design, needle crystals (raphides) of biogenic calcium oxalate monohydrate (COM, $CaC_2O_4{\cdot}H_2O$) contained in grape leaves were the focus of this study. The micrometric morphology and nanometric structures of COM in grape leaves were characterized to provide a hint that would clarify the specific biological crystal and bioinspired control of crystal growth.

Biogenic calcium oxalate observed in idioblasts is categorized into five types based on their morphology: prism, styloid, raphide, crystal sand, or druse.[10] Raphides—found in 24 orders, 46 families, and 797 species[13]—are needle-shaped COM crystals or amorphous calcium oxalates covered with organic chambers.[10,14–24] The morphology of raphides is classified into six forms by their cross-sectional shape, apical form, and internal structure.[21] In general, raphides are arranged as bundles in idioblasts and are thought to play a role in regulating the calcium concentration in plants and in defending against predators.[10,25–27] Although raphides in leaves of aloe and agave were judged to be single crystals of COM by electron diffraction,[28] the crystalline nature has not been sufficiently characterized in detail for other plants. In grapes, the raphide was suggested to be a rotational twin crystal with a longitudinal left–right partitioning.[29] In raphides of banana pseudostems and duckweed leaves, amorphous calcium oxalate was shown to exist as an aggregate of nanoparticles.[23,24,30] The organic chambers have been reported to include water-insoluble proteins with a strong affinity for calcium in water lettuce.[17] The presence of protein fibers has been demonstrated in banana

Department of Applied Chemistry, Faculty of Science and Technology, Keio University, 3-14-1 Hiyoshi, Kohoku-ku, Yokohama 223-8522, Japan.
E-mail: hiroaki@applc.keio.ac.jp

† Electronic supplementary information (ESI) available: A photo of a grape leaf, optical micrographs of idioblasts in a leaf, and SEM images of a cross section of a leaf (Fig. S1); SEM images and a schematic illustration of a bundle of raphides (Fig. S2); XRD pattern and Raman spectra of raphide bundles and standard COM (Fig. S3); SEM images of a raphide after dissolution of COM with EDTA solution and after removal of organic matter with calcination (Fig. S4); FTIR spectra of raphide bundles and standard COM (Fig. S5); TEM images and SAED patterns of raphides, and TEM and SEM images and schematic illustration of the same raphide shown in Fig. 5d in the main text (Fig. S6); optical micrographs and schematic illustrations indicating variation of morphology of raphide bundles (Fig. S7); an SEM image of a bundle of raphides after demineralization and TEM and SEM images of longitudinal sections of immature raphides (Fig. S8); TEM and enlarged SEM images of lateral sections of immature raphides (Fig. S9); optical micrographs of a bundle before and after decomposition into needles by a weak mechanical stimulation after removal of cytoplasm (Fig. S10); FTIR assignments of COM and protein in raphides and cellulose in Fig. S2 (Table S1). See DOI: https://doi.org/10.1039/d5ce00259a

pseudostems.[22] Because of their variety, the crystallinity, orientation, and organic constituents of raphides must be discussed in detail for specific species.

This article reports the sophisticated design, including the micrometric morphology and nanometric structures, of raphides in grape leaves, because details of the crystallinity of COM and the shape of organic chambers should be discussed in relation with the peculiar needle-like morphology. Furthermore, grapes, which are easy to cultivate, are advantageous for observing the formation process. Here, the crystallinity of COM for raphides in grape leaves was discussed with the relationship between the morphology and crystallographic orientation, and nanometric structures consisting of tiny particles. Fig. 1 shows schematic illustrations of the hierarchical architecture of a raphide. This research has arrived at accurate descriptions of the specular twin-like configuration regulated by the organic framework and the mesocrystal nature of the biological COM. Here, the essence of the elaborate structural design of biological crystals in plants was studied. The new scientific discovery will impact the evolution of science and technologies in the fields of biomineralization, crystal engineering, and bioinspired material processing.

Results and discussion

Micrometric feature of raphides

Fig. 2, S1 and S2 in the ESI† show macrometric arrangement of bundles of raphides in an idioblast of a grape leaf. The raphides are parallelly arranged as a bundle at the center region of an idioblast (Fig. 2a, c, f and g). Raphides were assigned to a monoclinic crystal of COM based on X-ray diffraction (XRD) patterns and Raman spectra (Fig. S3 in the ESI†). Slight variations in the Raman signals between raphides and standard COM suggest that distortion of the crystal lattice is present in the biogenic product.

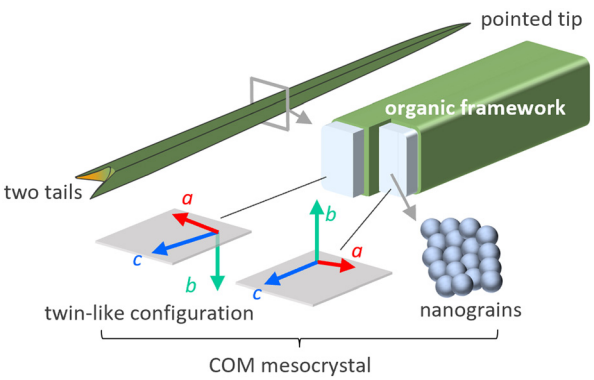

Fig. 1 Schematic illustration of the hierarchical architecture of a raphide in grape leaves. At the micrometric scale, a raphide with a pointed tip and two tails is regarded as having a twin-like chiral configuration of COM divided by an organic central wall and covered with an organic enveloping membrane. At the nanometric scale, the COM of a raphide has a mesocrystalline structure that consists of small grains ~10 nm in diameter with a distorted single-crystal nature.

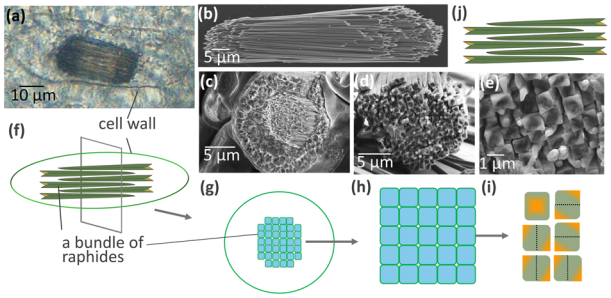

Fig. 2 Optical micrograph (a), SEM images (b–e), and schematic illustrations (f–j) for a bundle of raphides in an idioblast. Green, light blue, and yellow parts indicate the organic framework, the COM crystal, and the inside faces of tails of a needle, respectively.

Fig. 3a–d shows that a raphide is a rectangular needle with a pointed tip and two tails. On the cross section of the idioblast, the rectangular needles in the bundle are stacked in a tetragonal lattice (Fig. 2d, e, h and i). On the side view of the raphides, the top direction of the rectangular needles is random in a bundle (Fig. 2b and j).

As shown in previous articles,[29] twofold rotational symmetry along the longitudinal central axis was observed on the tails of a raphide (Fig. 3e and f). The tails are located only at the upper left and lower right positions relative to the line dividing the raphide to left and right (Fig. 3i). This means that the raphide has a form chirality and only one

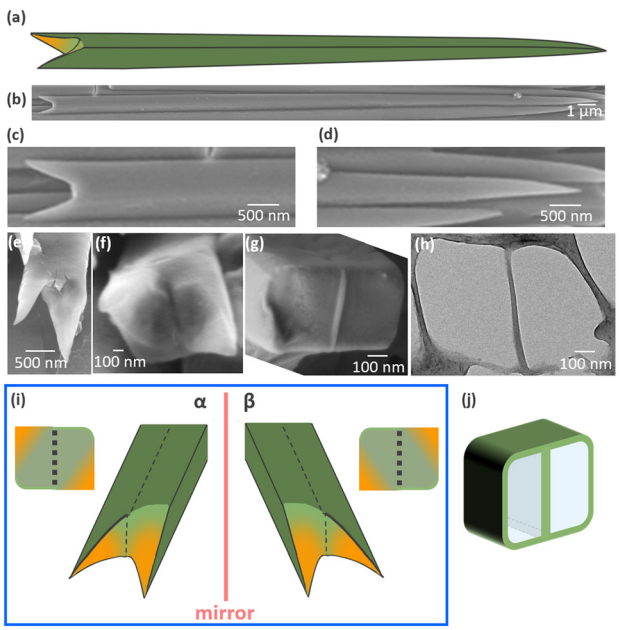

Fig. 3 SEM (b–g) and TEM (h) images and schematic illustrations (a, i and j) for a raphide that is a rectangular needle with a pointed tip and two tails (a–e). The left and right parts are divided by a center wall (f–h and j). The tails are located only at the upper left and lower right positions relative to the line dividing the raphide into left and right (i-α). Raphides with tails located at the lower left and upper right position (i-β) were not observed.

enantiomer is present, which is known as homochirality. A similar chirality was reported on crystal sands of COM.[31,32]

From the SEM and TEM images of the cross section of a raphide (Fig. 3g, h and j and S4 in the ESI†), the left and right parts are divided by a center wall. Fig. 4a and b shows a SEM image for a raphide end with two tails after the partial dissolution of COM with an ethylenediaminetetraacetic acid (EDTA) solution. We observed the organic framework as a chamber and the central wall that divides the COM into left and right portions. The presence of the organic frame consisting of a surrounding chamber and a central wall was confirmed by morphological change after calcination at 340 °C in air (Fig. 4c and d). The central trench and the smooth surface were formed around the raphide end through removal of the organic matter. After the EDTA and heat treatments, SEM images confirmed that the main body of a raphide was also divided along the backbone of a needle by the organic central wall (Fig. S4 in the ESI†). The amide signals were observed in FTIR spectra (Fig. S5 in the ESI†) for the raphide after the complete dissolution of COM. This suggests that the organic framework is mainly composed of proteins. The raphide surface was reported to be covered by an organic chamber[10,14–24] composed of water-insoluble proteins with a strong affinity for calcium in water lettuce[20] and cytoskeletal proteins in banana.[24] Here, we found that the chiral needles in grape leaves are divided by an organic wall with coverage by an enveloping organic membrane. However, we do not have direct evidence for the perfect separation of the left and right portions of the twin-like structure with the central wall.

Nanometric feature of twin-like COM

From the location of the two tails and the extinction pattern of polarized light microscope images, the raphide was deduced to be a rotational twin splitting longitudinally in its left–right direction.[29] However, the crystallographic orientation and detailed structure of the twin crystal have not been clarified using diffraction techniques. Here, we revealed details of the chiral morphology with organic framework of raphides. The left and right parts of a raphide are sectioned by the organic central wall (Fig. 3 and 4). This means that the raphide is not a simple twin crystal, which is composed of two single crystals directly attaching to the twin boundary.

The crystallographic orientation of the raphide was analyzed by electron diffraction. Fig. 5 and S6 in the ESI† show TEM and SEM images, an SAED pattern, and schematic illustrations of the two tails of a raphide. The diffraction patterns from three parts of raphides were categorized into two sets of the COM crystal lattice. From the assignment of the crystal zone axes ([010] and [0–10]) (Fig. 5a–c and S6a–f†), a raphide was deduced to have a rotational twin-like configuration that consists of two parts and have the same *c*-axis direction and the inverse directions of *a* and *b* axes.

The tails are located at the upper left and lower right positions relative to the wall. The SAED pattern from the two tails was also categorized into two sets of the COM crystal lattice (Fig. 5d–f). From the SEM observation of the same tails, the left and right tails are located at the upper and lower sides, respectively (Fig. S6g–i†). These results indicate that the *b* axes are parallel to the central wall. Moreover, the zone axis for the diffraction spots from the right tail was assigned to [010] (Fig. 5g–i). Therefore, the raphide is

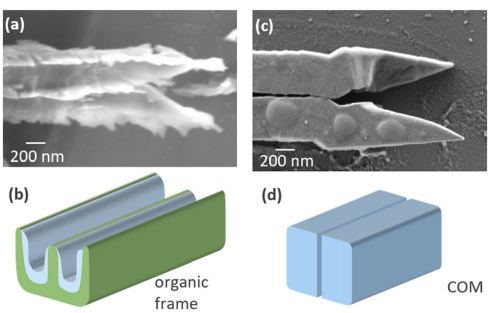

Fig. 4 SEM images (a and c) and schematic illustrations (b and d) of a raphide end with two tails after the dissolution of COM with an EDTA solution (a and b) and after the removal of organic matter with calcination at 340 °C in air (c and d).

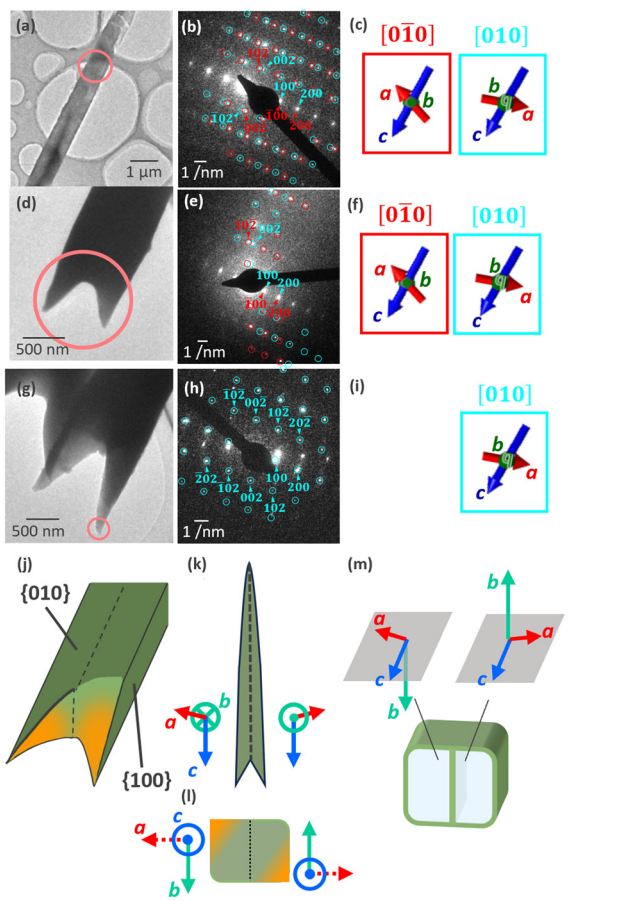

Fig. 5 TEM (a, d and g) images, an SAED pattern (b, e and h), crystallographic directions (c, f and i), and schematic illustrations (j–m) of the main body after partial demineralization with EDTA and the two tails of a raphide.

deduced to have the configuration shown in Fig. 5j–m. Here, the top and side faces are assigned to {010} and {100}, respectively.

As shown in Fig. 6a and b, we found that COM consists of nanograins ~10 nm in diameter on the cross section of a raphide. The presence of nanograins was confirmed by TEM images of powder that was decomposed from a raphide in ethanol with ultrasonication (Fig. 6c–f). The direction of the same crystal lattice was found to deviate at the grain boundary. Thus, the nanograins were separated by low-angle grain boundaries. Since the single-crystalline feature of the left and right parts was observed with SAED patterns (Fig. 5), the raphides are categorized as mesocrystal, which is an ordered assembly of separated nanograins in the same crystallographic direction. The mesocrystal is generally observed for a wide variety of biominerals.[1–4,6–8,33] The granular texture of mesocrystal was shown to inhibit crack propagation.[34–36] Here, we observed that the lattice directions of the nanograins are slightly deviated at the boundaries between nanograins. The distortion of the mesocrystal structure is advantageous for improving stiffness of the needles.[8,37]

Regulation of COM by an organic framework

We placed the bottom wall of the organic framework (Ca: 0%, C: 10.0% N: 2.8% O: 7.7%) that is regarded as a ribbon on a silicon substrate after the demineralization of a raphide (Fig. 7a). The organic membrane was immersed in a supersaturated solution of calcium oxalate to promote

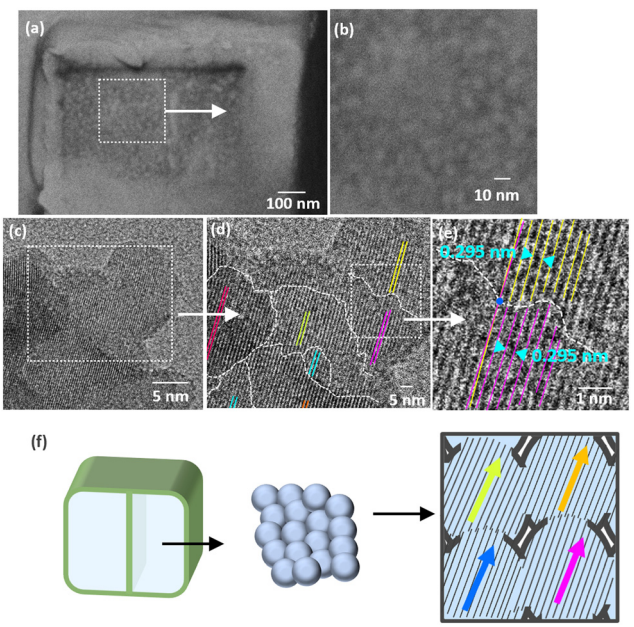

Fig. 6 Enlarged SEM images (a and b) of the cross section of a raphide, TEM images (c–e), and schematic illustrations (f) of COM nanograins. The lattice was assigned to (200), (–202), (023), or (0–23) of COM in (d and e). Different colored lines indicate slightly different directions of the lattices.

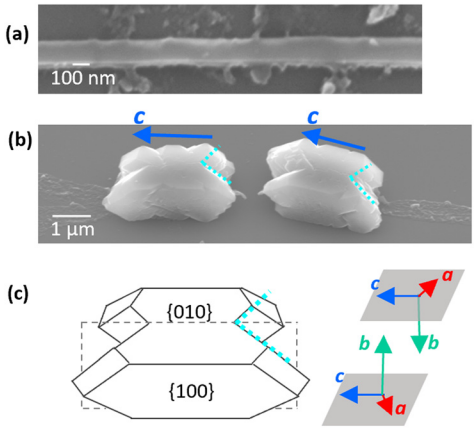

Fig. 7 SEM images of the organic membrane before (a) and after (b) the crystal growth of COM in a supersaturated solution. A schematic illustration of a twin of COM (c).[40] Aqua lines indicate the recessed area of a twin crystal.

remineralization. We found the formation of polyhedral blocks on the substrate (Fig. 7b). The specific form (Fig. 7c) and composition (Ca: 9.7%, C: 28.7% O: 56.0%) as evaluated by energy-dispersive X-ray spectroscopy (EDS) suggest that twin crystals of COM ($CaC_2O_4{\cdot}nH_2O$) are arranged on the *c*-axis on the ribbon. Thus, the organic framework induces the nucleation and initiates the growth of twin COM in a specific orientation. The role of the crystal chamber was studied using a partially demineralized raphide.[17] This experiment clearly demonstrated the function of the organic framework. In this case, however, the central wall is absent in the twin. The ordered array of carboxy groups of a protein chain was shown to promote the nucleation of calcium carbonate.[38] Moreover, the nucleation of a specific crystal phase of calcium carbonate was reported to be induced on an organic substrate by the similarity of ion distances between calcium sites on a crystal plane and carboxy groups of a polymeric molecule.[39] Since directionally controlled COM was formed on the organic membrane as shown in Fig. 7, the ion distance between carboxy groups on the membrane is inferred to be similar to that of calcium sites on the {010} of COM. Therefore, the particular configuration of COM is assumed to be constructed by the organic framework. However, further structural characterization of the proteins is needed to discuss the molecular interaction for clarification of the directional growth of twin-like COM.

Organic substances, such as organic chambers and mucus, in the idioblast are thought to play an important role in the formation of raphides. Fig. S7 in the ESI† shows development of bundles of raphides in grape leaves. We found that winding strings changed into straightened rods in bundles. Organic chambers were reported to be formed in the initial stage and COM then grew in them.[15,16,18–20] Winding shapes of the organic framework were observed after the removal of inside COM (Fig. S8a in the ESI†). Thus, the winding strings suggest the presence of organic

chambers without crystals that are regarded as a product in the initial stage (Fig. S7a–c in the ESI†). Short needles and sharpening tips were found as immature raphides (Fig. S8b–e in the ESI†). The formation of these short needles in the organic frames would straighten the morphology of the bundles gradually (Fig. S7c, f, i and j in the ESI†). We observed the organic framework on the cross section of a bundle of immature raphides (Fig. S9 in the ESI†). The crystal was found to be insufficiently staffed in the frame. The present observation supports the belief that crystal growth inside the organic frames is previously produced as a bundle.

Discussion of the twin-like configuration of tapered needles with a mesocrystal structure

Bundles of raphides were easily decomposed into needles by weak mechanical stimulation after the removal of cytoplasm (Fig. S10 in the ESI†). Thus, single needles would play a role in defending against predators. A tapered morphology with a pointed tip is advantageous for sticking the needle to the body of predators for the protection of plant leaves. Stringers of honeybee have barbs, which are similar in shape to the two tails of raphides.[41] The presence of barbs was reported to make the strings difficult to extract from targets. Thus, two tails could make irreversible the sticking of the needle in the body to enhance damage to predators. The symmetric configuration of the twin-like structure is favarable to the formation of two tails at the end of a crystal. Moreover, the central wall and the distorted mesocrystal structure would prevent crack propagation[42] and improve stiffness of the needles.[8,37] Thus, the twin-like configuration is also deduced to be useful for strengthening the raphides.

Conclusion

Raphides with a pointed tip and two tails in grape leaves were characterized as having a twin-like chiral configuration of calcium oxalate monohydrate divided and covered with an organic frame. Since small grains ~10 nm in diameter were found in the crystalline body, the raphide is deduced to be a mesocrystal with a distorted single-crystal nature. The crystal growth of calcium oxalate monohydrate is controlled by an initially produced organic frame under the construction of raphides in specific cells.

Experimental section

Sample preparation

Leaves of grape trees (*Vitis labrusca*) that were cultured at our laboratory located in Yokohama, Japan were used as samples. For optical micrograph, grape leaves were immersed in a water–ethanol (30 : 70) solution for 12 h. After washing in purified water, leaves were then immersed in a 2% NaClO solution for 48 h. After being washed with purified water and ethanol, the leaves were mounted on a microscope slide and observed by light microscopy (Keyence, VHX-1000). Fresh leaves were also fixed in a mixture of 2% glutaraldehyde, 4% paraformaldehyde, and 0.1 M cacodylate buffer (pH 7.4), washed with 0.1 M cacodylate buffer (pH 7.4) overnight at 4 °C, and then incubated in 1% osmium tetroxide with 0.1 M cacodylate buffer (pH 7.4) for 2 h at room temperature. After being dehydrated with an ethanol series, the samples were embedded in epoxy resin. The specimens were sectioned with a diamond knife using ultramicrotome (Leica, EM UC7). Thick sections (about 2 μm) were stained with 0.1% toluidine blue and observed by light microscopy (Nikon, Eclipse Ci). Ultra-thin sections (about 80 nm) were stained with uranyl acetate and Reynolds' lead citrate and observed by TEM (JEOL, JEM-1400plus, 100 kV). For cryo-SEM observation (Hitachi, S-3400, 5 kV), sections of leaves were quickly frozen in slush nitrogen and then etched at −95 °C.

Leaves were soaked and crushed in ethanol with a blender to obtain raphides. After the exchange of the liquid media into 8 M CsCl and 4 mM $CaCl_2$ solution (density 1.8 g cm^{-3}), raphides were obtained as a precipitate by centrifugation due to the density difference (cellulose: 1.5 g cm^{-3} and COM: 2.2 g cm^{-3}). Raphides were stored in a 4 mM $CaCl_2$ solution after removal of CsCl by centrifugation. Before characterization, stored raphides were fixed on a substrate by dropping the stored liquid after drying and subsequent flushing with purified water and ethanol.

Characterization

SEM-EDS (JEOL, JSM-7100F, 5 kV; JSM-IT700HR/LA, 5 kV; Zeiss, Merlin compact, 1–1.5 kV) was used to characterize the morphology of the surface and the cross section of the samples. Raphides were fractured on a carbon tape by manipulating a tungsten needle with a micromanipulator (Micro Support, Sampling Station). To remove organic matter and COM, raphides on a silicon substrate were heated at 340 °C in air and were etched with an EDTA solution, respectively.

XRD (Bruker, D8 Advance), TEM (FEI, Tecnai, 120 kV) with electron diffraction, and Raman spectroscopy (Renishaw, InVia Raman Microscope) were used to identify the crystalline phase and orientation of raphides. To analyse SAED patterns, ReciPro, which is diffraction simulation software, was used.[43] IR spectra (JASCO, FT/IR-4200) of untreated and EDTA-etched raphides were obtained by the KBr method. Nanograins were isolated from raphides by ultrasonification in acetone for TEM observation (FEI, Tecnai G2, 200 kV).

Remineralization and crystal growth on organic frame

Raphides on a silicon substrate were immersed in a 10 mM EDTA solution for 48 h to obtain organic frames. The organic substrate was immersed in a supersaturated solution for COM by mixing a 20 mM $Na_2C_2O_4$ solution and a 20 mM $CaCl_2$ solution. Resultant deposition was immersed in purified water and ethanol for 10 s, and then dried at 25 °C.

Data availability

The authors declare that the data supporting the findings of this study are available within the paper and its ESI† file. Raw data files are available from the corresponding author upon reasonable request.

Author contributions

H. I. supervised the project. R. T., H. W., Y. O., and H. I. designed the experimental procedure of structure analysis. R. T. analysed the macro- and microstructures and performed crystal growth on the organic frames. All authors reviewed the manuscript.

Conflicts of interest

There are no conflicts to declare.

Acknowledgements

This work was supported by JSPS KAKENHI grant number 21H01627 (23K21040).

Notes and references

1 Y. Oaki and H. Imai, *Adv. Funct. Mater.*, 2005, **15**, 1407–1414.
2 Y. Oaki, A. Kotachi, T. Miura and H. Imai, *Adv. Funct. Mater.*, 2006, **16**, 1633–1639.
3 Z. Deng, Z. Jia and L. Li, *Adv. Sci.*, 2022, **9**, 2103524.
4 H. P. Yu and Y. J. Zhu, *Chem. Soc. Rev.*, 2024, **53**, 4490.
5 K. Sato, A. Yamauchi, N. Ozaki, T. Ishigure, Y. Oaki and H. Imai, *RSC Adv.*, 2016, **6**, 109168–109173.
6 K. Izumida, M. Takasaki, R. Fujimaki, Y. Nagai, Y. Oaki, K. Naito, Y. Tanaka, S. Shimode, T. Toyofuku and H. Imai, *CrystEngComm*, 2022, **24**, 2446–2450.
7 R. Fujimaki, N. Suzuki, K. Kimoto, Y. Nagai, Y. Oaki, S. Shimode, T. Toyofuku and H. Imai, *Sci. Rep.*, 2022, **12**, 2848.
8 N. Nishio, S. Sugiyama, T. Yoshimura, R. Terasaki, M. Takasaki, Y. Oaki, T. Sasaki and H. Imai, *CrystEngComm*, 2023, **25**, 4213–4218.
9 M. Yamaguchi, Y. Nakamura, H. Watanabe, K. Kimoto, Y. Oaki, S. Shimode and H. Imai, *Sci. Rep.*, 2024, **14**, 13481.
10 V. R. Franceschi and P. A. Nakata, *Annu. Rev. Plant Biol.*, 2005, **56**, 41–71.
11 H. He, D. Li, X. Li and L. Fu, *Crystallogr. Rev.*, 2024, **30**, 31–60.
12 E. Letavernier, D. Bazin and M. Daudon, *Healthcare*, 2023, **11**, 2.
13 N. S. Lawrie, N. M. Cuetos, F. Sini, G. A. Salam, H. Ding, A. Vancolen, J. M. Nelson, R. H. J. Erkens and G. Perversi, *AoB Plants*, 2023, **15**, 1–16.
14 A. P. Kausch and H. T. Horner, *Can. J. Bot.*, 1984, **62**, 1474–1484.
15 M. A. Webb, *Plant Cell*, 1999, **11**, 751–761.
16 M. A. Webb, J. M. Cavaletto, N. C. Carpita, L. E. Lopez and H. J. Arnott, *Plant J.*, 1995, **7**, 633–648.
17 X. Li, D. Zhang, V. J. Lynch–Holm, T. W. Okita and V. R. Franceschi, *Plant Physiol.*, 2003, **133**, 549–559.
18 C. J. Prychid, R. S. Jabaily and P. J. Rudall, *Ann. Bot.*, 2008, **101**, 983–995.
19 G. X. Xu, C. Tan, X. J. Wei, X. Y. Gao and H. Q. Zheng, *Protoplasma*, 2011, **248**, 257–266.
20 A. M. A. Mazen, D. Zhang and V. R. Franceschi, *New Phytol.*, 2003, **161**, 435–448.
21 V. Raman, H. T. Horner and I. A. Khan, *J. Plant Res.*, 2014, **127**, 721–730.
22 X. Li, W. Zhang, J. Lu, L. Huang, D. Nan, M. A. Webb, F. Hillion and L. Wang, *Chem. Mater.*, 2014, **26**, 3862–3869.
23 W. Zhang, J. Chi, L. Ma and L. Wang, *Cryst. Growth Des.*, 2018, **18**, 1155–1161.
24 W. Zhang, Y. Fan and J. Chi, *J. Exp. Bot.*, 2024, **75**, 2470–2480.
25 P. A. Nakata, *Plant Sci.*, 2003, **164**, 901–909.
26 K. Konno, T. A. Inoue and M. Nakamura, *PLoS One*, 2014, **9**, e91341.
27 C. Tu, M. Zhang, M. Wu, M. Liu and W. Ke, *Ecotoxicol. Environ. Saf.*, 2024, **282**, 116728.
28 Y. Ishii, *J. Electron Microsc.*, 1992, **41**, 53–55.
29 H. J. Arnott and M. A. Webb, *Int. J. Plant Sci.*, 2000, **161**, 133–142.
30 E. Weber, A. Verch, D. Levy, A. N. Fitch and B. Pokroy, *ChemistrySelect*, 2016, **1**, 132–135.
31 N. Bouropoulos, S. Weiner and L. Addadi, *Chem. – Eur. J.*, 2001, **7**, 1881–1888.
32 A. Levy–Lior, S. Weiner and L. Addadi, *Helv. Chim. Acta*, 2003, **86**, 4007–4017.
33 E. Zolotoyabko, *Adv. Mater. Interfaces*, 2017, **4**, 1600189.
34 X. Li, Z. H. Xu and R. Wang, *Nano Lett.*, 2006, **6**, 2301–2304.
35 T. Sumitomo, H. Kakisawa, Y. Owaki and Y. Kagawa, *J. Mater. Res.*, 2008, **23**, 3213–3221.
36 Z. Deng, L. Chen and L. Li, *J. Mech. Behav. Biomed. Mater.*, 2023, **137**, 105538.
37 Y. Y. Kim, J. D. Carloni, B. Demarchi, D. Sparks, D. G. Reid, M. E. Kunitake, C. C. Tang, M. J. Duer, C. L. Freeman, B. Pokroy, K. Penkman, J. H. Harding, L. A. Estroff, S. P. Baker and F. C. Meldrum, *Nat. Mater.*, 2016, **15**, 903–910.
38 F. A. Davila-Hernandez, B. Jin, H. Pyles, S. Zhang, Z. Wang, T. F. Huddy, A. K. Bera, A. Kang, C. Chen, J. J. De Yoreo and D. Baker, *Nat. Commun.*, 2023, **14**, 8191.
39 A. Kotachi, T. Miura and H. Imai, *Chem. Mater.*, 2004, **16**, 3191–3196.
40 A. Millan, *Cryst. Growth Des.*, 2001, **1**, 245–254.
41 Z. L. Zhao, H. P. Zhao, G. J. Ma, C. W. Wu, K. Yang and X. Q. Feng, *Biol. Open*, 2015, **4**, 921–928.
42 J. Song, C. Fan, H. Ma, L. Liang and Y. Wei, *Acta Mech. Sin.*, 2018, **34**, 143–150.
43 Y. Seto and M. Ohtsuka, *J. Appl. Crystallogr.*, 2022, **55**, 397–410.